Hindawi
Journal of Sensors
Volume 2024, Article ID 4696031, 10 pages
https://doi.org/10.1155/2024/4696031

Research Article

Blood Oxygen Saturation Estimation with Laser-Induced Graphene Respiration Sensor

Ana Madevska Bogdanova,[1] **Bojana Koteska**,[1] **Teodora Vićentić**,[2] **Stefan D. Ilić**,[2] **Miona Tomić**,[3] **and Marko Spasenović**[2]

[1]*Faculty of Computer Science and Engineering (FCSE), "Ss Cyril and Methodius" University, Rugjer Boshkovikj 16, Skopje 1000, North Macedonia*
[2]*Center for Microelectronic Technologies, Institute of Chemistry, Technology and Metallurgy, National Institute of the Republic of Serbia, University of Belgrade, Njegoševa 12, Belgrade 11000, Serbia*
[3]*School of Electrical Engineering, University of Belgrade, Bulevar Kralja Aleksandra 73, Belgrade 11000, Serbia*

Correspondence should be addressed to Ana Madevska Bogdanova; ana.madevska.bogdanova@finki.ukim.mk

Received 15 November 2023; Revised 10 January 2024; Accepted 16 January 2024; Published 29 January 2024

Academic Editor: Carlos Michel

Measuring blood oxygen saturation (SpO_2) is crucial in a triage process for identifying patients with respiratory distress or shock, since low SpO_2 levels indicate compromised hemostability and the need for priority treatment. This paper explores the use of wearable mechanical deflection sensors based on laser-induced graphene (LIG) for SpO_2 estimation. The LIG sensors are attached to a subject's chest for real-time monitoring of respiratory signals. We have developed a novel database of the respiratory signals, with corresponding SpO_2 values ranging from 86% to 100%. The database is used to develop an artificial neural network model for SpO_2 estimation. The neural network performance is promising, with regression metrics mean squared error = 0.184, mean absolute error = 0.301, root mean squared error = 0.429, and R-squared = 0.804. The use of mechanical respiration sensors in combination with neural networks in biosensing opens new possibilities for noninvasive SpO_2 monitoring and other innovative applications.

1. Introduction

Real-time health monitoring has the potential to profoundly alter the strategies employed in the prevention and management of diseases, particularly in triage situations with a high number of casualties, by facilitating prompt identification of the most severely injured individuals. In particular, the ability to monitor vital parameters, such as heartbeat, respiration, blood oxygen saturation (SpO_2), and blood pressure in real-time can save lives in those critical situations. Timely detection of anomalies in these parameters can provide early warning of medical emergencies, enabling healthcare professionals to take swift action and prevent unwanted outcomes [1].

Measuring SpO_2 is an important part of the triage process, as it is used to establish patient hemostability and to prioritize patient treatment based on the severity of each patient's condition [2]. The main reason for measuring this vital parameter is detecting victims or patients with severe respiratory distress or shock: patients in shock may have decreased tissue perfusion and low SpO_2 levels. The common way of measuring SpO_2 is by utilizing a photoplethysmography (PPG) sensor, i.e., by analyzing the light absorption characteristics of oxygenated and deoxygenated hemoglobin. However, there are some drawbacks to using PPG for SpO_2 measurements. One limitation is that PPG-based SpO_2 measurements may not be as accurate as those obtained from arterial blood gas analysis or pulse oximetry using dedicated sensors. PPG signals can also be affected by motion artifacts, ambient light interference, and variations in skin pigmentation or thickness [3].

Wearable mechanical deflection sensors have been shown to be an effective and reliable method for real-time monitoring of respiration, with potential applications in sleep apnea

monitoring, exercise physiology, and respiratory disease management [4–6]. Laser-induced graphene (LIG), an emerging material recently used for mechanical deflection sensors, is an excellent candidate for wearable respiration monitoring [7–10]. LIG is a type of graphene that is created by irradiating a polymer or other organic material with a laser [11]. The laser energy causes the material to carbonize and transform into a graphene-like structure. Graphene, a single layer of carbon atoms arranged in a hexagonal lattice, has unique properties that make it attractive for sensor applications [12]. Its high electrical conductivity, large surface area, and biocompatibility have led to research exploring the use of graphene-based sensors for various biomedical purposes [13, 14]. In our prior publication [15], we established a correlation between LIG-obtained signals and heartbeat parameters using the HeartPy toolkit implemented in Python [16].

In this paper, we investigate the use of wearable mechanical deflection sensors made of LIG, used as respiration monitors, for SpO_2 estimation as an alternative for oximeters with PPG signals, with a vision of using such sensors as components of integrated wearable patch-like multisensor devices, since there is a relationship between the magnitude of respiratory peaks and the oxygen concentration [17]. Our main goal is to create an integrated patch-like sensor capable of delivering the four crucial hemostability parameters (heart rate, respiratory rate, blood pressure, and SpO_2). These parameters are vital for monitoring the medical condition of patients or injured individuals in emergency situations [18]. This patch-like sensor serves as the sole device required for continuous monitoring of the biosignals, eliminating the need for at least three separate devices (oximeter, blood pressure device, ECG/PPG sensors).

The LIG sensors employed in this paper detect changes in mechanical deflection, such as chest or abdominal movements, which are used to measure respiration rate and volume. The sensors are noninvasive and can be easily integrated into wearable devices such as belts or patches, making them suitable for continuous monitoring of respiratory parameters, as well as other vital parameters [15]. An artificial neural network (ANN) is used to extract SpO_2 from respiration measurements, making use of the fact that oxygenation and respiration are closely interconnected physiological processes. A direct link between real-time respiration signals and SpO_2, such as the one that we make, has not been demonstrated before. The use of LIG in biosensors for the real-time SpO_2 estimation and prediction opens the door to novel applications that are not available with other types of sensing devices. This paper also elaborates on the creation of a novel database consisting solely of LIG-obtained respiratory signals with corresponding SpO_2 references in the range of 86%–100%.

In the past, researchers have demonstrated the use of graphene in prototype flexible photodetectors for measuring heart rate, arterial oxygen saturation (SpO_2), and respiratory rate [19]. Such prototypes are of good use for wearable respiration monitoring using optical technology; however, they suffer from the same disadvantages as traditional PPG technology. Similarly, there is a plethora of research focused on SpO_2 estimation using machine learning and deep learning models, as well as calculations based on PPG signals [20, 21], but none based on real-time respiration signals. Our approach overcomes some of the mentioned drawbacks of using PPG signals, as well as the need for preprocessing of PPG signals when used in ML/ANN/DNN models [22].

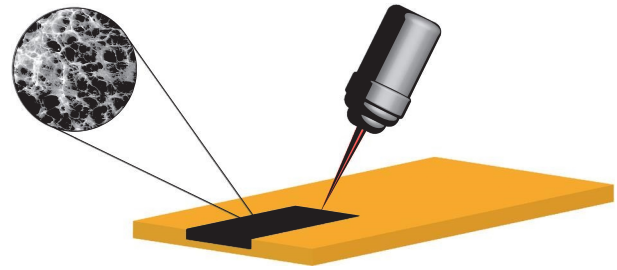

Figure 1: Production of laser-induced graphene by CO_2 laser beam.

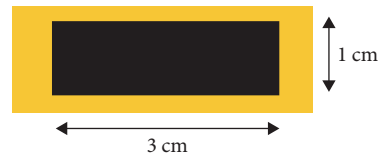

Figure 2: A sketch of sensor geometry. Black represents graphene, and yellow represents PI tape.

The paper is organized as follows: in Section 2, we describe the production of the LIG sensor and material characterization (Section 2.1). We also describe the novel LIG database (Section 2.2) and the used ANN model for SpO_2 estimation (Section 2.3). In Section 3, we elaborate on the obtained results, presenting a discussion in Section 4. Section 5 presents concluding remarks and several ideas for future work.

2. Materials and Methods

2.1. Graphene Sensor Production, Characterization, and Respiration Monitoring. LIG was produced by scanning a CO_2 laser beam across the surface of polyimide tape, as illustrated in Figure 1 [23]. The laser used was DBK FL-350, with a maximum power of 60 W. The power was set to 18%, the scanning speed was 400 mm/s, and the scanning resolution was 800 DPI.

The devices were formed by laser-writing LIG in the shape of rectangles with dimensions 1×3 cm, as in Figure 2. The graphene was transferred to double-sided adhesive medical tape (Duplomed 8411, Lohmann, GmbH, Neuwied, Germany). Raman spectra of the samples were recorded with a DXR Raman microscope (Thermo Fisher Scientific, Waltham, MA, USA). The samples were excited with a diode laser at a wavelength of 532 nm and a power of 10 mW, focused on a 2.1 μm spot on the surface. Spectra were obtained as averages of three measurements from different positions on the sample (10 exposures, 10 s each per position). The recorded Raman spectra were treated to correct the fluorescence background using a 5th-order polynomial baseline correction method built-in the Omnic software (OMNIC for Dispersive Raman 9.2.41.). SEM with EDS was done with a PhenomProX scanning electron microscope (Phenom, Thermo Fisher Scientific, Waltham, MA, USA). XRD analysis was carried out on a D8 Advance Eco

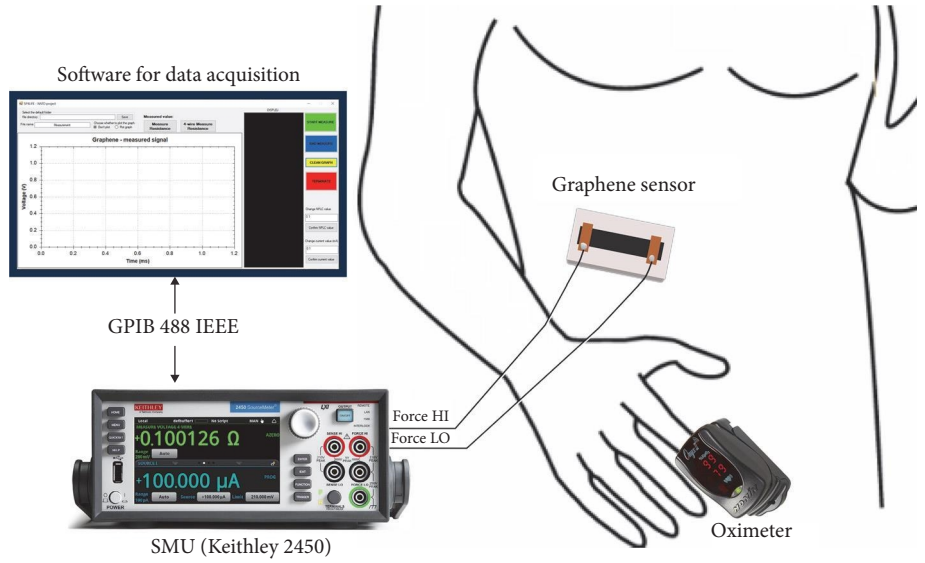

Figure 3: Experimental setup for tracking respiration using an SMU Keithley 2450, a graphene sensor, a pulse oximeter, and a desktop computer.

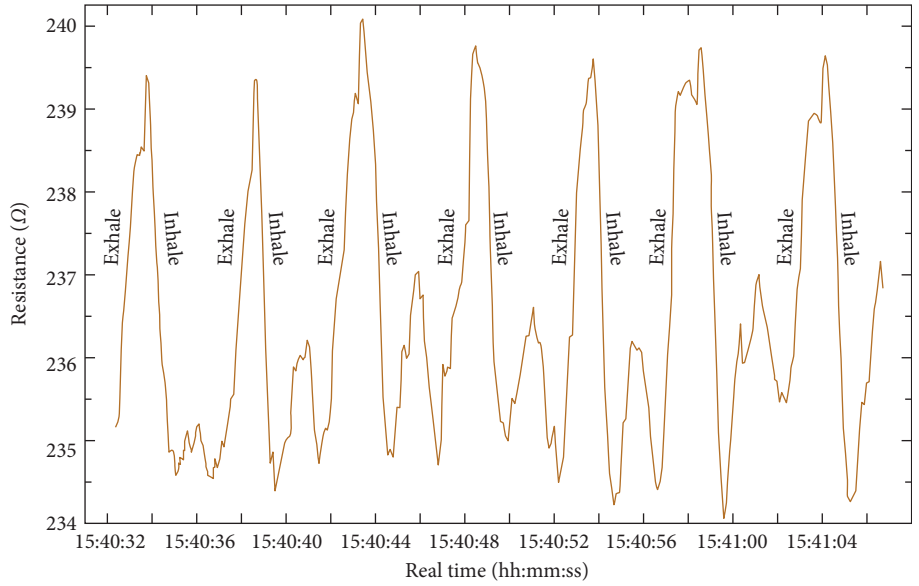

Figure 4: Resistance variation in time, as breathing is monitored with an LIG-based device.

diffractometer with Cu Kα radiation ($\lambda = 0.15{,}406$ nm, Bruker, Germany). Electrical contacts were made to the LIG by attaching conductive copper tapes at the device's ends. Wires were soldered to copper tapes and connected to the measuring device. Such contacting provides ohmic contact to the graphene. The sensor was attached to the body by adhesion of the medical tape to the skin in the chest area.

The experimental setup consisted of a one-channel source-measure unit (SMU) Keithley 2450, a desktop computer that controls the measuring device and acquires data using a Windows application written in C#, a graphene sensor attached to the body using medical tape and connected with cables to the SMU Keithley 2450, and a commercial Onyx II oximeter (Nonin Medical, Plymouth, MN, USA) placed on a finger of a volunteer subject (Figure 3). The specified precision of the oximeter of +/−2% is sufficient to evaluate the concept of applying machine learning in combination with mechanical deflection sensors to predict SpO_2 from respiration data.

Measurements were performed in the constant current mode with the current set to 0.1 mA, and the voltage was measured over a period of 30 s. The placement of the graphene sensor on the torso allows for the capture of respiratory signals, which provide valuable information regarding the breathing pattern (Figure 4). The measurement shown in Figure 4 starts with exhalation, followed by a sequence of seven breaths, as labeled on the graph. Although we measure voltage while keeping the current fixed, it is more intuitive to

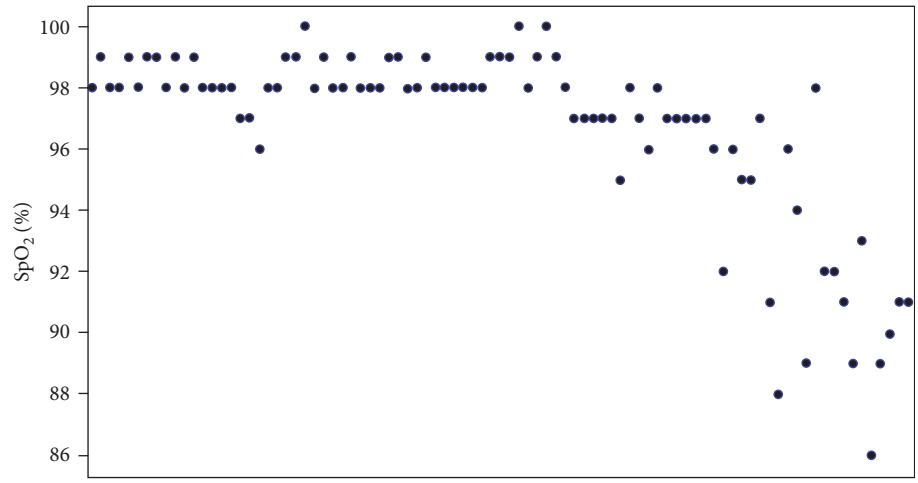

Figure 5: Scatter plot of the SpO_2 values obtained and added to the database.

plot the resistance than the voltage. Hence, in Figure 4, we convert the measured voltage to resistance using the simple linear relation $V = I^*R$, and we plot resistance over time during breathing.

2.2. LIG Database. Respiration data were collected from three healthy volunteer subjects, as our primal interest is the triage process of healthy injured victims of mass victim incidents. The number of subjects relates to already published studies—one and three subjects, respectively [24, 25]. During our measuring, the subjects sat in a chair and breathed normally while wearing the LIG sensor. Simultaneously, reference SpO_2 measurements were obtained using the oximeter. The signals were recorded and conducted with approval from the Ethical Committee. We created a novel database consisting of 89 measurements of respiratory signals. The majority of measurements in the novel database exhibit normal oxygen saturation ($SpO_2 \geq 95\%$), but we also recorded some values below 95%, even down to 86%, as depicted in Figure 5. To record data with SpO_2 less than 90%, i.e., the critical level [22], we applied the breath-holding technique [26, 27]. The subjects held their breath for 30, 45 s, 1, or 2 min, resuming breathing after that. The first 30–40 s of breathing after holding breath were recorded. Including SpO_2 values lower than 95% in the database is important for applications in clinical and casualty situations in which patients may exhibit low SpO_2. We have qualitatively observed that, although intense motion may cause signal artifacts, the artifacts do not survive the postprocessing treatment. Moreover, these sensors are expected to be used in cases when wounded or sick individuals are lying still and not moving.

As some commercial SpO_2 sensors provide readings every 10 s [28], we aimed at similarly fast measurements by utilizing 20–30 s of the LIG sensor signals in our analysis. By utilizing an approach that allows for signals of different temporal durations, we aim to expand on the range of opportunities for applying our neural network algorithm to respiration signals.

Unlike PPG signals typically used for SpO_2 estimation, the LIG-obtained signals did not require preprocessing such as normalization, Butterworth band-pass filtering, or Hampel decision filtering. The LIG-obtained respiratory signals were used raw and unprocessed for the estimation of SpO_2.

In the process of generating an ANN learning model for SpO_2 prediction, a crucial step is to generate a list of features from the respiratory signals. These features serve as input vectors for the model and play a vital role in training the network to identify significant patterns related to SpO_2 estimation. By extracting relevant features from the respiratory signals, the ANN can learn to recognize patterns and establish relationships between the input signals and SpO_2 levels. This feature extraction step is essential for capturing the relevant information present in the respiratory signals and facilitating accurate predictions of SpO_2. These extracted features can then be analyzed and utilized to characterize the respiratory pattern [7, 8].

Using empirical analysis, a set of 10 common features was selected to describe the LIG respiratory signals. These specific features were chosen based on their significance in capturing essential characteristics of the respiratory signals. The NumPy [29] and SciPy [30] Python libraries were used to support the features calculation.

Table 1 presents the elaborated respiratory features in a structured way, together with a short explanation. The comprehensive definitions and explanations for all features are available in the Appendix section.

2.3. ANN Model. This research employed a supervised learning approach by building an ANN to estimate the SpO_2 value as a regression problem. The ANN is designed to output a single value representing the predicted SpO_2 value, while the input is a matrix containing the 10 respiratory features extracted from the input signal.

The dataset was divided into a training set, consisting of 70% of the data (62 measurements), and a testing set containing the remaining 30% (27 measurements). Prior to splitting the dataset, a standardization process was applied to ensure consistent scaling and facilitate effective training and evaluation of the model.

Table 1: Common features of the respiratory signals.

Amplitude features	
Peak amplitude	Maximum value of the respiratory signal
Trough amplitude	Minimum value of the respiratory signal
Mean amplitude	Average value of the respiratory signal
Standard deviation	Measures how far the signal fluctuates from the mean
Time-domain features	
Breath duration	Duration of each individual breath in the respiratory signal
Respiratory rate	Number of breaths per minute, calculated using frequency analysis or peak detection methods
Variability features	
RRV mean	Average value of respiratory rate variability across a specific time period
RRV std	Provides information about the degree of variability in the respiratory rate intervals
Shape features	
Rise time	Refers to the time it takes for the signal to transition from a baseline or resting state to a peak or maximum value
Fall time	Refers to the time it takes for the signal to transition from a peak or maximum value back to a baseline or resting state

The implementation of the ANN involved the use of the Keras API written in Python, which runs on top of the TensorFlow machine learning platform. The architecture of the employed ANN in this study is illustrated in Figure 6.

The Keras library's sequential module was employed to build a sequence of ANN layers that are stacked in consecutive order. To specify the number of neurons, the Dense Keras module is used to define each layer. As depicted in Figure 6, the learning neural network is fully connected, comprising several hidden layers with a particular number of neurons and one output layer with only one neuron that predicts the SpO_2 value.

To perform calculations within each neuron, we employed the rectified linear unit (ReLU) function as the activation function, which is the most widely used activation function [31]. The ReLU function produces an output of zero if the input value is less than zero; otherwise, it is equal to the provided input value. To compute the loss, we used mean squared error (MSE) as it is the most commonly used loss function for regression [32].

To determine the optimal accuracy, we conducted a tuning process on the ANN model, exploring different combinations of the "epoch" and "batch_size" values. Specifically, we used grid search cross-validation to test various values for these hyperparameters. The "batch_size" parameter refers to the number of training examples used in a single forward/backward pass, while 'epochs' indicates the number of times the learning algorithm runs through the entire training dataset.

To assess the accuracy of the model, we used standard regression metrics: mean absolute error (MAE), MSE, root mean squared error (RMSE), root mean log squared error (RMLSE), and R-squared (R^2).

MAE represents the average absolute difference between the predicted and actual values, providing a measure of the model's overall accuracy. MSE implements the average squared difference between the predicted and actual values, emphasizing larger errors. RMSE is the square root of MSE, which provides a more interpretable metric in the original scale of the target variable. R^2, also known as the coefficient of determination, measures the proportion of the variance in the target variable that can be explained by the model. A higher R^2 value indicates a better fit of the model to the data. By considering these metrics, we can assess the model's accuracy, precision, and ability to explain the variability in the target variable, aiding in the evaluation and comparison of different ML/ANN models.

3. Results

The Raman spectrum of LIG (Figure 7(a)) exhibits characteristic features of graphene. Prominent D and G bands appear at 1,338 and 1,590 cm^{-1}, respectively. The G peak indicates the presence of sp^2 carbon atoms, while the D peak signals defects in graphene. The 2D peak at 2,700 cm^{-1} is attributed to second-order zone boundary phonons [33, 34].

The XRD pattern of LIG (Figure 7(b)) shows a significant peak at $2\theta = 26.5°$, suggesting the presence of a graphitic phase with an inter-planar distance of 3.4 Å corresponding to the (002) plane [11]. The interplanar distance is calculated using Bragg's law for the first-order diffraction, X-ray wavelength of 1.54 Å, and an incident beam angle of $\theta = 13.25°$. A characteristic peak at $2\theta = 14.8°$ indicates the production of graphite oxide, while the peak at $2\theta = 22.4°$ is formed due to the formation of reduced graphene oxide, caused by oxygen contamination on the polyimide films during the laser induction process [35].

To examine both the morphology and elemental composition of LIG, SEM-EDS analysis was conducted (Figure 7(c)). The produced LIG film displays a distinctive foam-like appearance with porous structures, a result of the rapid release of gaseous products during the laser-induction process [36]. The sample was further used to assess the elemental composition of LIG (Figure 7(d)). EDS analysis reveals the presence of carbon, oxygen, silicon, and chlorine, while the atomic percentage of carbon equals 95.25%. These findings indicate that negligible oxidation occurred during the graphene formation process.

Figure 8 illustrates the training loss during the training process. The decreasing trend observed in the training loss curve indicates an improvement in the model's performance over time. This suggests that the model is effectively learning and adapting to the training data without overfitting. This outcome is desirable as it indicates the model's ability to generalize well to unseen data and make accurate predictions beyond the training set. The decreasing trend in the training loss curve provides confidence in the model's learning

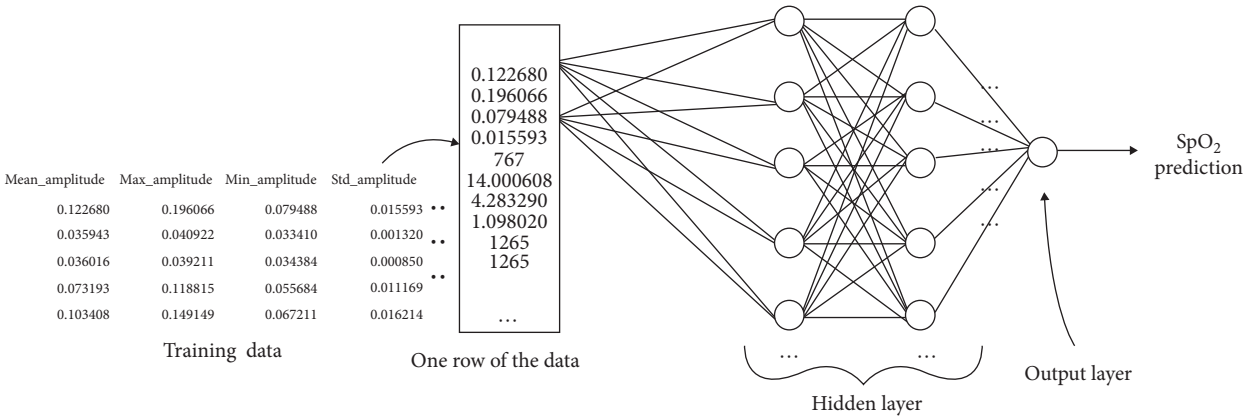

Figure 6: ANN architecture.

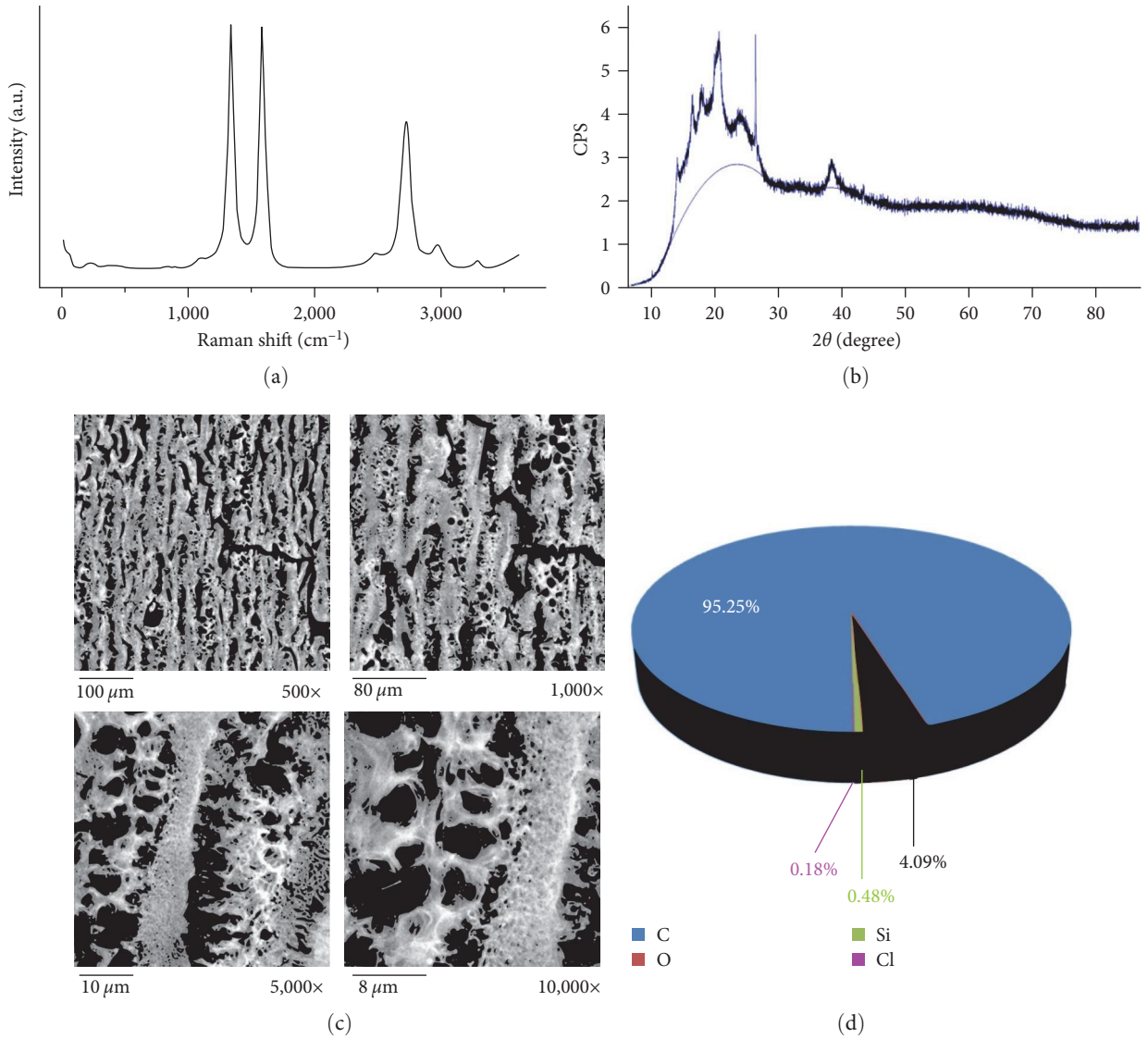

Figure 7: LIG characterization: (a) Raman spectrum; (b) XRD pattern; (c) SEM images at different magnification levels; (d) EDS analysis.

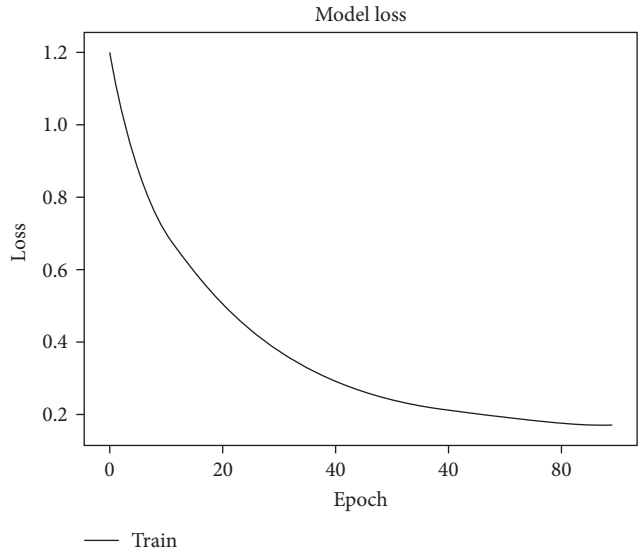

Figure 8: Model training loss curve.

process and its potential effectiveness in predicting SpO_2 values. We tested the optimal number of epochs by performing experiments with different numbers of epochs. The validation loss ceases to improve as the number of epochs increases beyond 90, which was the final number of epochs that we used.

Table 2 presents the actual and predicted SpO_2 values from the testing set containing 27 measurements.

Table 3 shows results from the model's performance evaluation metrics in predicting SpO_2 from respiratory signals.

The ANN model's performance in predicting SpO_2 from respiratory signals yields promising results. The MSE of 0.184 suggests that, on average, the model's predictions deviate from the actual SpO_2 values by a relatively small squared difference. The MAE value of 0.301 indicates that the model's average absolute difference between predicted and actual SpO_2 values is also reasonably low. The RMSE value of 0.429, derived from the MSE, provides a more interpretable metric in the original scale of SpO_2, showing that the model's predictions align well with the true values. Furthermore, the R^2 value of 0.804 demonstrates that approximately 80.4% of the variance in SpO_2 can be explained by the model, indicating a good fit to the underlying patterns in the data. These results collectively demonstrate the effectiveness and accuracy of the presented ANN learning model in predicting SpO_2 from LIG-obtained respiratory signals.

Table 2: Comparison of actual and predicted SpO_2 values for the testing dataset.

Actual SpO_2	Predicted SpO_2	Absolute difference
99	99.4	0.4
97	96.5	0.5
98	98.3	0.3
98	97.8	0.2
100	98.2	1.8
98	97.8	0.2
97	97.3	0.3
96	97.5	1.5
98	98.7	0.7
99	98.4	0.6
99	98.7	0.3
99	98.2	0.8
98	98	0.0
92	90.6	1.4
91	91.4	0.4
98	97.6	0.4
89	93.8	4.8
98	97.1	0.9
89	90.4	1.4
98	98.4	0.4
98	97.9	0.1
98	99.7	1.7
98	98.6	0.6
99	97.4	1.6
97	95.7	1.3
99	97.9	1.1
96	95.4	0.6
96	95.1	0.9

Table 3: Obtained regression metrics.

Metric	Result
MSE	0.184
MAE	0.301
RMSE	0.429
R^2	0.804

4. Discussion

Our research aimed to explore the feasibility of utilizing LIG sensors as an alternative SpO_2 estimator by leveraging the nature of LIG-obtained signals as respiratory signals. The impact of the demonstrated results is twofold. First, the results demonstrate that LIG sensors can be used to measure respiration in real time, which opens doors for the use of low-profile wearable LIG-based patches for medical and wellness applications. Second, we have shown that temporal respiration data obtained from signals of chest expansion and contraction during breathing can be used as input to an ANN that outputs SpO_2 with high precision and correctness.

The underlying physiological relationship between SpO_2 and respiration action is rooted in the process of oxygen transfer and circulation within the body. When we breathe, oxygen enters the respiratory system and is transported to the bloodstream, where it binds to hemoglobin in red blood cells. This oxygenated blood is then distributed throughout the body, ensuring the delivery of oxygen to various tissues and organs [37]. Given this connection, by analyzing respiratory signals captured by the LIG sensors, we aimed to

investigate their potential to serve as indicators for estimators of SpO_2 levels.

Earlier work has shown that simple RR measurements do not correlate well with SpO_2 in patients [38]. Nevertheless, here we have shown that the utilization of the chosen 10 respiratory features as input vectors in our ANN model overcomes this hurdle, with excellent matching to reference measurements of SpO_2.

Although our study has used real-time respiratory data acquired with LIG sensors, we believe that the model could be applicable to different real-time respiratory data obtained from various types of sensors. Given that the number and type of available sensors are growing at a fast pace with the development of new technology [39], our model will certainly find numerous applications in wearable and bedside devices.

Direct comparisons with other studies that estimate SpO_2 by ML/ANN models using LIG-obtained signals as input are not possible due to the lack of existing literature and databases with LIG-obtained respiratory signals and SpO_2 references. Future work may encompass analysis of publicly available databases containing respiratory signals and SpO_2 measured by other means, such as radio frequency signals [40]. For example, the National Institute of Health (USA) has compiled databases with various health parameters, including respiration signals and SpO_2, measured during sleep [41].

One notable advantage of our approach is the flexibility in the length of the respiration signal as an input vector for the ANN. Also, the feature extraction process maintains the integrity of the respiratory information. Furthermore, our research revealed that preprocessing the LIG-obtained respiratory signals is unnecessary, in contrast to the preprocessing required for PPG signals used in SpO_2 estimation. This finding holds great significance for practical applications with time-critical implications.

The compactness of the presented ANN model is a significant advantage since it provides quick and timely SpO_2 level estimations. The model can be deployed in emergency situations as an integral component of a telemedicine system [18].

In terms of future work, there is potential to enhance the novel database by including more data, particularly focusing on SpO_2 values below 90%, which may be obtained in a hospital setting from unhealthy patients. As indicated in Table 2, the largest disparity between the actual and predicted SpO_2 values is observed for the value of 89%. By expanding the dataset to incorporate a wider range of SpO_2 values, including those below 90%, the performance and accuracy of the ANN model can be further refined.

5. Conclusion

This paper explores the use of wearable mechanical deflection sensors made of LIG for estimating SpO_2 as an alternative to PPG-based oximeters. These sensors measure mechanical deflection, such as chest or abdominal movements, to estimate respiration rate and volume. The LIG sensors are affixed to the subject's chest to enable real-time monitoring of respiratory signals. An ANN model is built to estimate SpO_2 from the respiratory measurements, leveraging the close relationship between oxygenation and respiration. To facilitate SpO_2 estimation, we have created a unique database comprising respiratory signals and corresponding SpO_2 values ranging from 86% to 100%. The neural network's performance demonstrates promise, as evidenced by regression metrics such as MSE of 0.184, MAE of 0.301, RMSE of 0.429, and R^2 of 0.804. The integration of mechanical respiration sensors with ANNs in biosensing presents exciting possibilities and the potential of using LIG sensors in SpO_2 estimation with high precision and accuracy.

Appendix

The first four features from the 10 features described in Section 2.2 represent "Amplitude" features. In respiratory signals, the term "amplitude" refers to the magnitude or intensity of the variations observed in the signal waveform. Amplitude represents the difference between the baseline or resting state and the peak values of the respiratory signal. The following four amplitude features were identified:

Peak amplitude of the sinusoidal respiratory waveform is the maximum positive deviation from its zero reference level;

Trough amplitude is the lowest part of the respiratory signal. It represents the minimum value reached by the signal during the exhalation phase;

Mean amplitude refers to the average magnitude or intensity of the variations observed in the signal waveform over a certain period of time. It represents the average difference between the baseline or resting state and the peak values of the respiratory signal;

Standard deviation, in this case, measures how far the signal fluctuates from the mean.

The following two features belong to the time domain in signal processing:

Breath duration is the duration of one breath in the measured sequence;

Respiratory rate, RR, is calculated as the number of breaths per minute, usually obtained by frequency analysis or peak detection methods. We calculate RR by the latter.

The next two are variability features:

Respiratory rate variabilities (RRVs) are the mean variations within the respiratory rhythm. Normal breathing exhibits a relatively constant rate and tidal volume that together constitute normal respiratory rhythm. However, variations within this respiratory rhythm are labeled as RRV [42]. RRV is a useful predictor of the deterioration of a patient's health. RRV Mean is calculated as the average value of respiratory rate variability across a specific time period;

RRV Std is the standard deviation or spread of the respiratory rate intervals around the mean value. A higher RRV Std indicates greater variability and a wider range of interval values [43].

The last two features are shape features. In respiratory signals, these values refer to characteristics of measurements

that describe the overall shape or waveform pattern of the respiratory signal:

Rise time in respiratory signals is defined as the time during which airway pressure builds up from a baseline toward a preset maximum value. A short rise time will allow instantaneous delivery of flow at the start of a breath cycle, resulting in an immediate rise in pressure to a preset level [44];

Fall time is defined as the time that airway pressure takes to return from a maximum value toward a baseline or resting state.

Data Availability

The data used in this study are available upon request. Please contact Bojana Koteska at bojana.koteska@finki.ukim.mk for access to the dataset.

Conflicts of Interest

The authors declare that they have no conflicts of interest.

Acknowledgments

This work was supported in part by the NATO Science for Peace and Security Program under project SP4LIFE, number G5825. This work was supported in part by the Ministry of Science, Technological Development and Innovation of the Republic of Serbia, grant number 451-03-47/2023-01/200026.

References

[1] S. J. Na, R.-E. Ko, M. G. Ko, and K. Jeon, "Automated alert and activation of medical emergency team using early warning score," *Journal of Intensive Care*, vol. 9, Article ID 73, 2021.

[2] M. Benson, K. L. Koenig, and C. H. Schultz, "Disaster triage: START, then SAVE—a new method of dynamic triage for victims of a catastrophic earthquake," *Prehospital and Disaster Medicine*, vol. 11, no. 2, pp. 117–124, 1996.

[3] M. Ghamari, D. Castaneda, A. Esparza, C. Soltanpur, and H. Nazeran, "A review on wearable photoplethysmography sensors and their potential future applications in health care," *International Journal of Biosensors & Bioelectronics*, vol. 4, no. 4, Article ID 195, 2018.

[4] A. Rasheed, E. Iranmanesh, W. Li et al., "An active self-driven piezoelectric sensor enabling real-time respiration monitoring," *Sensors*, vol. 19, no. 14, Article ID 3241, 2019.

[5] S. W. Park, P. S. Das, A. Chhetry, and J. Y. Park, "A flexible capacitive pressure sensor for wearable respiration monitoring system," *IEEE Sensors Journal*, vol. 17, no. 20, pp. 6558–6564, 2017.

[6] H.-F. Hu, S.-J. Sun, R.-Q. Lv, and Y. Zhao, "Design and experiment of an optical fiber micro bend sensor for respiration monitoring," *Sensors and Actuators A: Physical*, vol. 251, pp. 126–133, 2016.

[7] H. Chen, S. Bao, J. Ma et al., "A wearable daily respiration monitoring system using PDMS-graphene compound tensile sensor for adult," in *2019 41st Annual International Conference of the IEEE Engineering in Medicine and Biology Society (EMBC)*, pp. 1269–1273, IEEE, Berlin, Germany, 2019.

[8] H. Huang, S. Su, N. Wu et al., "Graphene-based sensors for human health monitoring," *Frontiers in Chemistry*, vol. 7, Article ID 399, 2019.

[9] G. Cantarella, M. Madagalam, I. Merino et al., "Laser-induced, green and biocompatible paper-based devices for circular electronics," *Advanced Functional Materials*, vol. 33, no. 17, Article ID 2210422, 2023.

[10] Y. Pang, K. Zhang, Z. Yang et al., "Epidermis microstructure inspired graphene pressure sensor with random distributed spinosum for high sensitivity and large linearity," *ACS Nano*, vol. 12, no. 3, pp. 2346–2354, 2018.

[11] J. Lin, Z. Peng, Y. Liu et al., "Laser-induced porous graphene films from commercial polymers," *Nature Communications*, vol. 5, Article ID 5714, 2014.

[12] E. W. Hill, A. Vijayaragahvan, and K. Novoselov, "Graphene sensors," *IEEE Sensors Journal*, vol. 11, no. 12, pp. 3161–3170, 2011.

[13] J. Sharma, S. Sharma, Ajay, and L. K. Sharma, "Role of graphene in biomedical applications," *Materials Today: Proceedings*, vol. 63, pp. 542–546, 2022.

[14] H. Zhang, R. He, Y. Niu et al., "Graphene-enabled wearable sensors for healthcare monitoring," *Biosensors & Bioelectronics*, vol. 197, Article ID 113777, 2022.

[15] T. Vićentić, M. R. Rafajilović, S. D. Ilić et al., "Laser-induced graphene for heartbeat monitoring with HeartPy analysis," *Sensors*, vol. 22, no. 17, Article ID 6326, 2022.

[16] P. van Gent, H. Farah, N. van Nes, and B. van Arem, "Heartpy: a novel heart rate algorithm for the analysis of noisy signals," *Transportation Research Part F: Traffic Psychology and Behaviour*, vol. 66, pp. 368–378, 2019.

[17] Ø. Rasch-Halvorsen, E. Hassel, A. Langhammer, B. M. Brumpton, and S. Steinshamn, "The association between dynamic lung volume and peak oxygen uptake in a healthy general population: the HUNT study," *BMC Pulmonary Medicine*, vol. 19, Article ID 2, 2019.

[18] F. Lehocki, A. M. Bogdanova, M. Tysler et al., "SmartPatch for victims management in emergency telemedicine," in *2021 13th International Conference on Measurement*, pp. 146–149, IEEE, Bratislava, Slovakia, 2021.

[19] E. O. Polat, G. Mercier, I. Nikitskiy et al., "Flexible graphene photodetectors for wearable fitness monitoring," *Science Advances*, vol. 5, no. 9, Article ID eaaw7846, 2019.

[20] I. B. Aguirregomezcorta, V. Blazek, S. Leonhardt, and C. H. Antink, "Learning about reflective PPG for SpO_2 determination using machine learning," *Current Directions in Biomedical Engineering*, vol. 7, no. 2, pp. 33–36, 2021.

[21] M. N. I. Shuzan, M. H. Chowdhury, M. E. H. Chowdhury et al., "Machine learning-based respiration rate and blood oxygen saturation estimation using photoplethysmogram signals," *Bioengineering*, vol. 10, no. 2, Article ID 167, 2023.

[22] B. Koteska, A. M. Bodanova, H. Mitrova, M. Sidorenko, and F. Lehocki, "A deep learning approach to estimate SpO_2 from PPG signals," in *Proceedings of the 9th International Conference on Bioinformatics Research and Applications*, pp. 142–148, IEEE, 2022.

[23] L. Wang, Z. Wang, A. N. Bakhtiyari, and H. Zheng, "A comparative study of laser-induced graphene by CO_2 infrared laser and 355 nm ultraviolet (UV) laser," *Micromachines*, vol. 11, no. 12, Article ID 1094, 2020.

[24] M. van Gastel, W. Verkruysse, and G. de Haan, "Data-driven calibration estimation for robust remote pulse-oximetry," *Applied Sciences*, vol. 9, no. 18, Article ID 3857, 2019.

[25] Z. H. Naeem, M. Youseffi, F. Sefat et al., "Design and development of a low cost pulse oximeter," *Journal of Physics: Conference Series*, vol. 1793, Article ID 012068, 2021.
[26] M. Chan, V. G. Ganti, J. A. Heller, C. A. Abdallah, M. Etemadi, and O. T. Inan, "Enabling continuous wearable reflectance pulse oximetry at the sternum," *Biosensors*, vol. 11, no. 12, Article ID 521, 2021.
[27] M. J. Parkes, "Breath-holding and its breakpoint," *Experimental Physiology*, vol. 91, no. 1, pp. 1–15, 2006.
[28] D. Shao, C. Liu, F. Tsow et al., "Noncontact monitoring of blood oxygen saturation using camera and dual-wavelength imaging system," *IEEE Transactions on Biomedical Engineering*, vol. 63, no. 6, pp. 1091–1098, 2016.
[29] C. R. Harris, K. J. Millman, S. J. van der Walt et al., "Array programming with NumPy," *Nature*, vol. 585, pp. 7825–7362, 2020.
[30] E. Jones, T. Oliphant, and P. Peterson, "Scipy: open source scientific tools for python," 2001.
[31] M. K. Büning, P. Kern, and C. Sinz, "Verifying equivalence properties of neural networks with ReLU Activation Functions," in *Principles and Practice of Constraint Programming*, vol. 12333 of *Lecture Notes in Computer Science*, pp. 868–884, Springer, 2020.
[32] M. Kolbæk, Z.-H. Tan, S. H. Jensen, and J. Jensen, "On loss functions for supervised monaural time-domain speech enhancement," *IEEE/ACM Transactions on Audio, Speech, and Language Processing*, vol. 28, pp. 825–838, 2020.
[33] L. M. Malard, M. A. Pimenta, G. Dresselhaus, and M. S. Dresselhaus, "Raman spectroscopy in graphene," *Physics Reports*, vol. 473, no. 5-6, pp. 51–87, 2009.
[34] A. C. Ferrari, J. C. Meyer, V. Scardaci et al., "Raman spectrum of graphene and graphene layers," *Physical Review Letters*, vol. 97, no. 18, Article ID 187401, 2006.
[35] S. Sharma, S. K. Ganeshan, P. K. Pattnaik, S. Kanungo, and K. N. Chappanda, "Laser induced flexible graphene electrodes for electrochemical sensing of hydrazine," *Materials Letters*, vol. 262, Article ID 127150, 2020.
[36] R. Ye, D. K. James, and J. M. Tour, "Laser-induced graphene," *Accounts of Chemical Research*, vol. 51, no. 7, pp. 1609–1620, 2018.
[37] J.-A. Collins, A. Rudenski, J. Gibson, L. Howard, and R. O'Driscoll, "Relating oxygen partial pressure, saturation and content: the haemoglobin-oxygen dissociation curve," *Breathe*, vol. 11, no. 3, pp. 194–201, 2015.
[38] W. R. Mower, C. Sachs, E. L. Nicklin, P. Safa, and L. J. Baraff, "A comparison of pulse oximetry and respiratory rate in patient screening," *Respiratory Medicine*, vol. 90, no. 10, pp. 593–599, 1996.
[39] M. Javaid, A. Haleem, S. Rab, R. P. Singh, and R. Suman, "Sensors for daily life: a review," *Sensors International*, vol. 2, Article ID 100121, 2021.
[40] P. Nguyen, X. Zhang, A. Halbower, and T. Vu, "Continuous and fine-grained breathing volume monitoring from afar using wireless signals," in *IEEE INFOCOM. 2016-The 35th Annual IEEE International Conference on Computer Communications*, pp. 1–9, IEEE, San Francisco, CA, USA, 2016.
[41] G.-Q. Zhang, L. Cui, R. Mueller et al., "The national sleep research resource: towards a sleep data commons," *Journal of the American Medical Informatics Association*, vol. 25, no. 10, pp. 1351–1358, 2018.
[42] F. J. Jacono and T. E. Dick, "Variability, measuring the spice of life," *Journal of Applied Physiology*, vol. 111, no. 2, pp. 1–4, 2011.
[43] J. Seely and P. Macklem, "Critical care London, England," 6 367, 2004.
[44] M. Amato and J. J. Marini, "Pressure-controlled and inverse-ratio ventilation," in *Principles and Practice of Mechanical Ventilation*, M. Tobin, Ed., pp. 251–272, McGraw-Hill, New York City, 2013.